A review and evaluation of the methodology for digitising 2D fracture networks and topographic lineaments in GIS

Romesh Palamakumbura[1], Maarten Krabbendam[1], Katie Whitbread[1] and Christian Arnhardt[2]

[1]British Geological Survey, The Lyell Centre, Research Avenue South, Edinburgh EH14 4AP, UK

[2]British Geological Survey, Nicker Hill, Keyworth NG12 5GG

Abstract. Understanding the impact of fracture networks on rock mass properties is an essential part of a wide range of applications in geosciences, from understanding permeability of groundwater aquifers and hydrocarbon reservoirs to erodibility properties and slope stability of rock masses for geotechnical engineering. However, gathering high quality, oriented-fracture datasets in the field can be difficult and time consuming, for example due to constraints on time or access (e.g. cliffs). Therefore, a method for obtaining accurate, quantitative fracture data from photographs is a significant benefit. In this paper we describe and evaluate the method for generating a series of digital fracture traces in GIS-environment, in which spatial analysis of a fracture network can be carried out. The method is not meant to replace the gathering of data in the field, but to be used in conjunction, and is well suited where fieldwork time is limited, or where the section cannot be accessed directly. The basis of the method is the generation of the vector dataset (shapefile) of a fracture network from a georeferenced photograph of an outcrop in a GIS environment. From that shapefile, key parameters such as fracture density and orientation can be calculated. Furthermore, in the GIS-environment more complex spatial calculations and graphical plots can be carried out such as heat maps of fracture density. There are a number of advantages to using a digital method for gathering fracture data including: time efficiency, generating large fracture network datasets, flexibility during data gathering and consistency of data.

1 Introduction

Fractures are the main pathways of fluid flow in rocks, and exert a strong influence on rock mass properties. The characterisation of fracture networks is an essential aspect of various applications in earth science, for example to understand and predict the behaviour of fluid flow in groundwater aquifers (Singhal and Gupta, 2010; Follin et al. 2014) and hydrocarbon reservoirs, and the erodibility and slope stability of rock masses. Fracture network data are essential for assessing future sites of nuclear waste repositories, predicting rock slope stability (Selby, 1982; Park et al., 2005) and understanding intact rock strength for engineering of infrastructure (Hoek and Brown, 1997; Zhan et al., 2017; Ren et al., 2017). For 2D fracture network analysis, there are a number fracture parameters that are widely used, including orientation, spacing, length, density/intensity and various connectivity proxies (summarised in Singhal and Gupta, 2010; Sanderson and Nixon, 2015; Peacock et al., 2016; Laubach et al., 2019). In this paper, we present and evaluate a 2D digital fracture network analysis method that is commonly in use in structural geology, and through numerous case studies we demonstrate the wider potential of

35   this method for other users, for example geotechnical engineers, groundwater modellers and
36   geomorphologists (Figure 1).

37
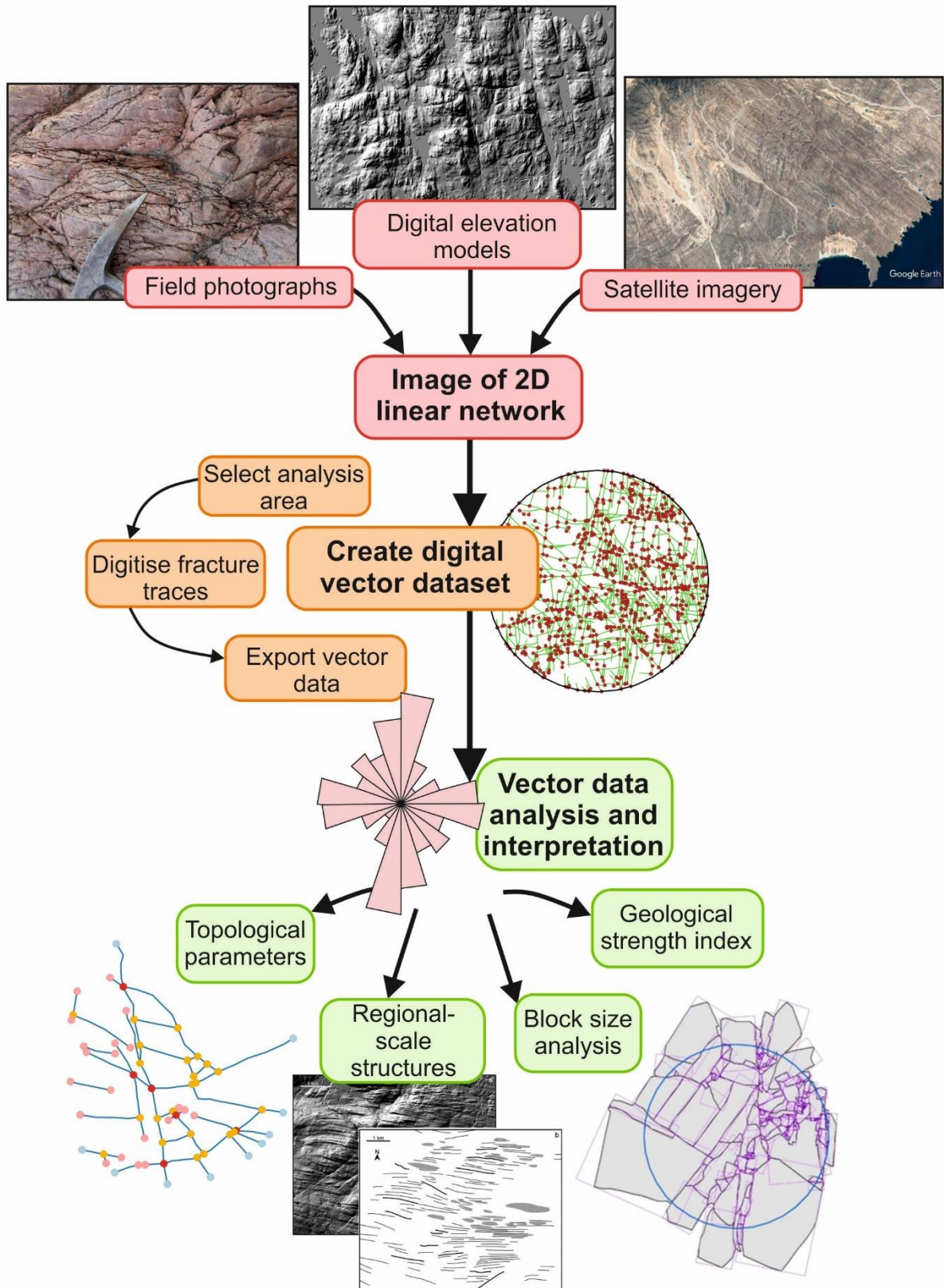
Figure 1: Flowchart providing an overview of the methodology used for digitising linear features, from preparing
an image, digitising the features to output of data. Digital elevation model examples are taken from Next
map © in Scotland, and the satellite image of Oman example is taken from Google Earth ©.

Fracture networks can be characterised in different dimensions using a number of approaches. 1D approaches include borehole fracture analysis and outcrop-based scanline surveys, typically represented by the number of fractures per unit length, i.e. frequency. 1D approaches are relatively rapid, but cannot directly constrain certain parameters such as fracture length and connectivity: if the fracture network is anisotropic (which is commonly the case), the characterisation is biased by the orientation of the scanline or the borehole ('orientation bias'; Singhal and Gupta, 2010; Zeeb et al. 2013b; Watkins et al. 2015b). 3D (really 2.5D) outcrop analysis using laser scanning provides a fuller analysis (e.g. Pless et al., 2015) but requires expensive equipment and is time-consuming in its processing. Unmanned Aerial Vehicles (UAVs) are used to generate high resolution images of an outcrop, with 3D information generated with techniques such as structure from motion (SfM) photogrammetry (Vasuki et al., 2014). True 3D characterisation is possible using CT scanning, but is restricted to very small samples (Voorn et al. 2015). As a compromise, many studies employ a 2D approach. Normally, this uses some form of characterisation within a circular window on a rock outcrop (Davies et al, 1996; Rohrbaugh et al. 2002; Watkins et al. 2015a). Generally, for 2D analysis a circular scanline or window approach is taken. In the former fractures intersecting the circular line are recorded, whereas in the latter fractures within the window area are recorded. Circular scanline methods are more rapid than full 2D circular window methods and have less length and orientation bias compared to 1D methods. A circular scanline can be used to calculate proxies for fracture density and length based on the ratio of the types of trace intersection (Mauldon et al. 2001). However, circular scanline methods lack the full analysis of a complete 2D circular window approach. Connectivity within two-dimensional fracture networks was parameterized by Manzocchi (2002), who characterised the different types of fracture intersections that can be used to characterise fluid percolation potential. A complete understanding of the fluid flow properties of a fracture network requires a broader understanding of 3D fracture network connectivity factors, such as fracture fill and aperture (Laubach et al., 2019).

Field-based 2D fracture network analysis is commonly carried out by using a circular 'chalk line' on and outcrop and measuring the fractures within the circular window. The benefit of the field-based method is an accurate data set that includes a range of parameters from fracture geometry (Singhal and Gupta, 2010) such as length and orientations, fracture network parameters (Singhal and Gupta, 2010) such as density and spacing, network topology (Sanderson and Nixon, 2019) such as percolation potential, and clustering and fracture character (Laubach et al., 2019) such as aperture and paragenesis history. However, there are a number of limitations when gathering fracture network data in the field. Firstly this can be very time consuming particularly when collecting large datasets across a large field

74 area. Secondly, some outcrops such as quarries or unstable cliffs may not be impractical or unsafe to

75 access for making fracture measurements. Thirdly, collecting fracture network data from larger fracture

76 networks of greater than 10 m can be challenging in the field, particularly when collecting fracture data

77 from an entire outcrop. Finally, more evolved modern fracture network analysis and modelling often

78 require a digital set of the fracture network traces.

79 The digital fracture trace method has been used for data collection in a range of structural geology

80 studies, including multiscale fracture network models (Strijker et al., 2012), the development of 3D

81 fracture models (Tavani et al., 2016; Menegoni et al., 2019) and developing discrete fracture networks

82 (DFNs) to model fluid flow (Bisdom et al., 2017). This methodology is used as the basis of data

83 generation in a broad range of structural studies, and this paper provides an evaluation of the method

84 that will be helpful to improve the quality of data collection.

85 Building on previous work (Krabbendam and Bradwell, 2014; Pless et al., 2015; Watkins et al., 2015a;

86 Krabbendam et al. 2016; Healy et al., 2017) we present and develop a method for capturing a 2D fracture

87 network as a digital (GIS) dataset from outcrop photographs. From this dataset, numerous key spatial

88 relationships and parameters can be calculated. The only equipment needed are a high-quality digital

89 camera, a measuring stick and GIS software (e.g. open source QGIS) for digitisation and analysis. This

90 method can also be applied to georeferenced (orthorectified) aerial photos, hillshaded DTMs and

91 satellite imagery for the characterisation of topographic lineaments. In addition, historic photos from

92 now-infilled excavations or quarries can be used, as long as the photos have a useable scale. The method

93 provides a relatively rapid and accessible way to generate accurate 2D fracture datasets and will be

94 beneficial for a wide range of users including engineering geologists and hydrogeologists.

95 **2 Digital 2D fracture analysis method**

96 The method in essence captures a set of digital traces (vectors) of a 2D linear feature network in a GIS

97 project from a georeferenced image. Here, we use open source GIS software (QGIS), making the

98 method accessible to all potential users. A number of open tools within QGIS can be used for more

99 advanced analysis of the digitised fracture network.

100 **2.1 Outcrop selection**

101 A suitable outcrop for digital fracture analysis must be first selected. Where spatial understanding of

102 the distribution or diversity of fracture characteristics in a region is an important element of study, the

103 implications of site selection choice on subsequent spatial analysis must also be considered. The outcrop

104 selected will depend on the nature of the study being undertaken and the type of fracture network

105 parameters required. It is important to consider whether the outcrop is representative of the rock mass

106 as a whole or whether multiple sites would better represent the diversity or distributions of fracture

107 characteristics. Outcrop selection has significant implications on the final results, i.e. whether the

108 outcrop is a proxy for wider-scale fracture network characteristics at depth or if it is the outcrop itself

109 that is being studied in isolation at the surface (Laubach et al 2019; Ukar et al 2019).

110

111 **2.2 Outcrop image preparation**

112 The first step is to prepare a suitable photograph or image of the outcrop to be analysed. The image can

113 be a photograph of a fracture network at outcrop of various scales from centimetres to 10s of metres. It

114 is important that the fractures can be clearly identified in the photograph, and that not too much of the

115 image is occupied by vegetation or broken ground (Figure 2a). It is important to include an accurate

116 and clearly identifiable scale; a strip of plywood with duct tape works very well. However, in some

117 dangerous outcrops (e.g. working quarries) this may be impractical and quarry machinery or other

118 features of known dimensions may be used as a scale in the photograph. The photograph should be

119 taken at right angles (or as much as possible) to the outcrop to minimise the issues created by a distortion

120 of the image. The camera should have a focal length of 35mm (analogue 35 mm equivalent) or longer,

121 to prevent further distortion. Horizontal outcrops should be photographed vertically to again minimise

122 the distortion of the fractures. Mounting the camera on a stick is useful to increase the distance and

123 capture a larger field of view (Figure 2b, c); or drones could also be used. For horizontal outcrops it is

124 convenient to orient the measuring stick accurately to the north, using a compass (Figure 2c), this will

125 help in capturing the correct orientations of the fractures.
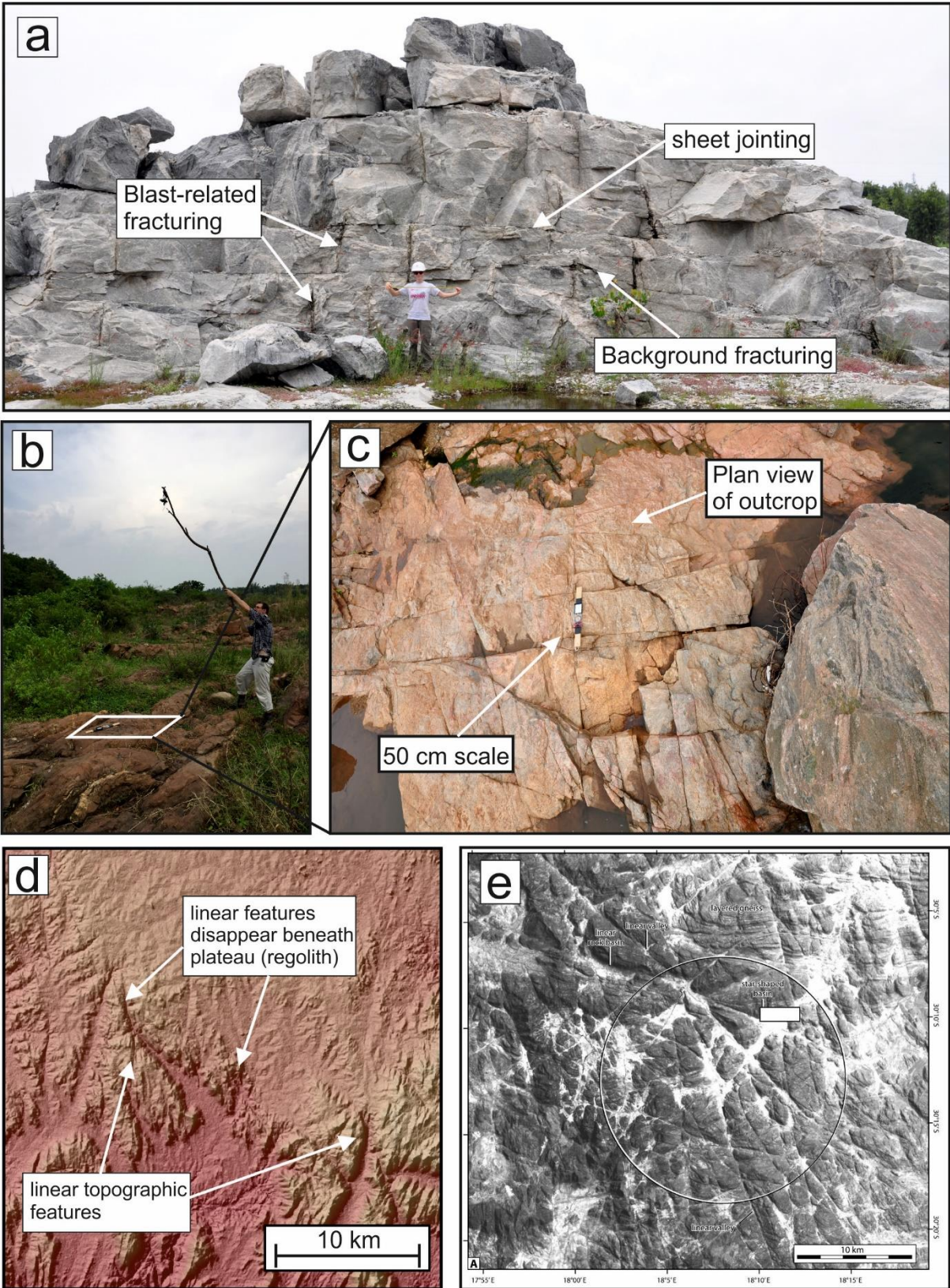
126
127 **Figure 2**: Examples of photographs and DEM images that can be used for digitising 2D linear features, including:
128 (a-c) photographs of fracture networks of various scale from southern India and improvised methods for taking
129 parallel photographs; (d) a DEM image from southern India of larger kilometre scale features that could also be
130 digitised; and (e) an aerial photography from Namibia (adapted from Krabbendam and Bradwell, 2014).

131

2.3 Georeferencing the images

To aid robust georeferencing, the photograph needs to have a square of known size (e.g. 1 x 1 m) embedded in it. This can be done by importing the photograph into a graphics software package (such as Inkscape), and drawing a square based on the scale included in the original photograph (Figure 3). The photograph with the embedded 1 x 1 m square is then imported into a new GIS project file. The GIS project file needs a projection in metres; we recommend a Mercator projection, (such as EPSG:3857). Within the GIS project, a 'vector grid' (fishnet grid) is created, with a grid extent that is larger than the imported photograph and with a vertical and horizontal spacing of 1.0 m. Finally, georeference the square on the photograph to a square on the fishnet grid, thus creating a georeferenced photograph within the GIS project (Figure 3a).
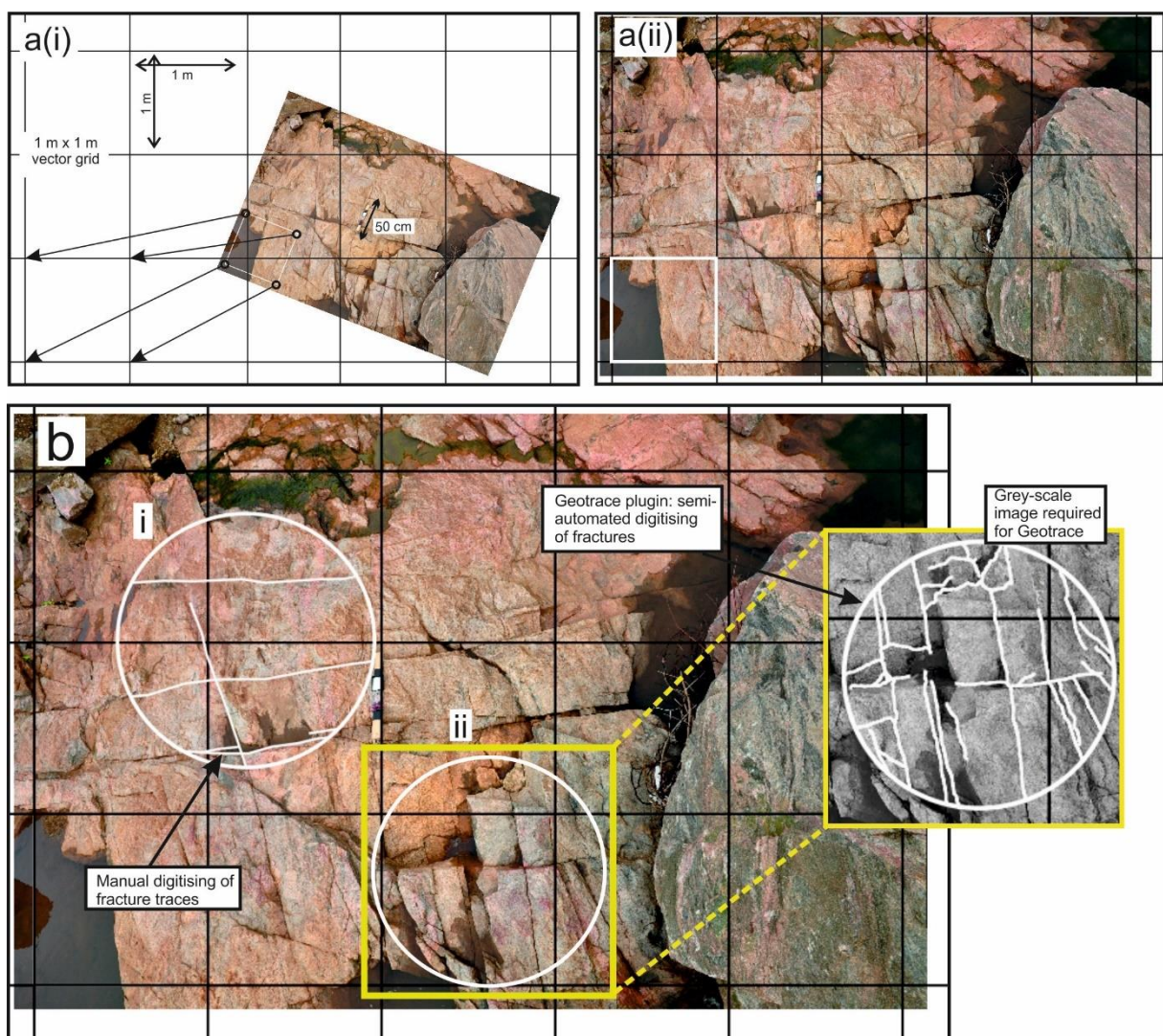
Figure 3: Images showing (a (i-ii)) how to georeference an image to a fishnet grid (black) from a square of a known scale (white); and (b) the tools available for digitising fractures in QGIS, including (i) a fully manual method; and (ii) a semi-automatic method such as Geotrace.

2.4 Using DEM, satellite and airphoto images

DEMs (Digital Elevation Models) (and their hill-shaded derivatives), satellite images and (orthorectified) aerial photographs commonly show good topographic lineaments that likely represent fracture zones, or master joints (Fig. 2d,e). Such imagery if georeferenced can be used directly without further preparation. It should be noted however that aerial photographs, DEMs and satellite images do not directly show fracture traces, rather they show the topographic expression of these. Thus, fracture density is likely to be underestimated, because fractures without topographic expression will not be captured. Figure 2d is an example of a DEM image from southern India showing kilometre-scale 2D topographic lineaments: in some parts lineaments are well developed, in other parts fracture zones have no expression and presumably occur beneath a continuous layer of regolith. Furthermore, such imagery is limited by the on-ground resolution, so that smaller-scale (smaller aperture) fractures may not appear. Hill-shade DEM images, as well as satellite imagery and aerial photographs have the problem of bias by a particular direction of illumination, so that lineaments of one orientation may be clearer than others. For DEMs, hill-shades derivatives with different illumination direction can be made; for satellite imagery, sometimes imagery taken at a different time of day are available. Lineaments in DEM images also have the problem of illumination, which may result in bias depending on the orientation of the lineament relative to the illumination orientation. Hence, for DEM-scale interpretations it is important to take a multi-data type approach (e.g. geological maps and satellite images) to guide digitisation, similar to that of Pless (2012).

2.5 Data capture

2.5.1 Select analysis window

Different 2D lineament analysis windows can be used with this method including line scanlines, areal sampling and circular windows. For each of these methods a different shaped sample window is required. For this create a line or polygon shapefile and digitise the area that is to be analysed. An example is shown in Figure 3b as two circular windows, in white, digitised onto a photograph in GIS. It is important to create a different id number for each shape that includes details of the photograph or image that is being digitised.

2.5.2 Digitise linear features

This step aims to create a series of digital line traces from the georeferenced image. Create a new line shapefile in the GIS project to hold the linear trace data. The shapefile needs to include an id column in the attribute table so that the linear traces can be associated with a specific window and photograph. Two methods can be used to create digital traces of the linear features. Firstly, the individual features can be digitised manually in the GIS project, using the "add line features" tool. Alternatively, the plugin tool "GeoTrace" can be used to semi-automate the digitising process. The GeoTrace plugin tool in

180 QGIS allows one to click on the start and end of each fracture and GeoTrace creates a line vector
181 between these points. For this method the photograph must be in grey scale, because the plugin follows
182 the linear feature based on low raster values and requires a sharp contrast between the feature and the
183 background. When digitising fracture traces it is important to only digitise in one orientation: if a
184 feature has multiple orientations along its length then multiple line segments should be digitised. Figure
185 3b is an example of both (i) manual digitisation and (ii) semi-automated digitisation with GeoTrace. In
186 both the manual and semi-automated methods, it is important that connecting fractures are properly
187 snapped against each other, and to the surrounding circular window.

188 A practical difficulty when analysing field outcrops will depend on whether the outcrop is natural or
189 anthropogenic. In a quarry or excavated section it can be challenging to distinguish natural joints from
190 those arising from quarrying processes, such as blast damage or drilling related fractures. Using field
191 observations, blast damage can be separated from natural joints (Figure 2a). Joints arising from blast
192 damage can easily be distinguished from natural joints as they do not fit with the overall fracture pattern
193 of the section, and are generally surrounded by small radiating fractures. The type of fractures digitised
194 will be depend on the study, and it is important to appreciate the wide range of processes causing
195 fractures that are dependent on the outcrop setting. Some basic initial observations in the field are
196 beneficial for making such distinctions at a later stage; hence, it is recommended that the outcrops that
197 are being analysed are always viewed in the field as well.

198 **2.6 Data output and further analysis**

199 The final step is to generate basic parameters and calculate dimensions from the digital traces of the
200 linear features. There are a number of different ways that the vector data can be analysed, which include:
201 1) using the field calculator in QGIS; 2) as an exported spreadsheet; or 3) using a programming language
202 such as Python or R to make calculations from the spreadsheet or directly from the shapefile.

203 Primary parameters can be calculated within the field calculator in the QGIS attribute table, including
204 length and orientation of individual fracture traces. The area of the circular window can also be
205 calculated in the attribute table using the field calculator. For further analysis, the attribute table
206 containing the primary fracture data (length, orientation and reference to the circular window) needs to
207 be exported as a spreadsheet, e.g. in CSV format. Fracture density (D) within the circular window can
208 now be calculated using total length of fractures (ΣL) within the area of the circular window (A),
209 following Singal & Gupta, (1999):

210 $D = \Sigma L/A$ (in m^{-1})   (1)

211 Fracture spacing (S) can be easily derived, as this is the reciprocal of fracture density, and is given by
212 (Singal & Gupta, 1999):

213 $S = A/\Sigma L$ (in m).   (2)

Other parameters, that can be derived from the digitised fracture network include the number and distribution of fracture intersections and block size. Fracture intersections (points) within the fracture network can be created as a separate point shapefile with the 'line intersection' tool. The digitised fracture traces can also be used to derive block size parameters, using the 'polygonise' tool to convert the line vectors into polygons. As before, parameters such as area can be derived using the field calculator in the attribute table and exported as a spreadsheet.

3 Case studies

Below we present a number of case studies that include fracture analysis for groundwater modelling; quantifying rock mass properties for engineering geology; and block size distribution to understand sediment erodibility that help demonstrate the potential broader uses of the digital GIS-based analysis of fracture networks.

3.1 Understanding fracture connectivity and permeability, southern India

Characterisation of fracture networks is an important aspect of trying to understand local and regional-scale aquifer properties such as connectivity and permeability. This type of understanding is particularly relevant for groundwater studies in fractured 'hard-rock' aquifers, where fractures are the primary water stores and pathways (e.g. Stober and Bucher, 2007; Singal and Gupta 2010). An example is given here of the Peninsular Gneiss in the Cauvery Catchment in southern India. The groundwater properties of the Cauvery Catchment has been an area of ongoing research (Maréchal et al 2006, Perrin et al 2011, Collins et al. 2020) due to the spatial and temporal variability of groundwater availability and the impact that this has on local communities. Two contrasting basement fracture networks can be identified (Figure 4a-b): firstly, one massive gneiss with few fractures, dominated by a widely spaced 'background jointing' and sheeting joints close to the surface, and secondly 'fracture zones' that are characterised by a very dense fracture network.

Length-weighted rose plots show the variation in orientation of fractures (in a vertical section) in the two identified domains. In the massive gneiss the fractures are generally orientated sub-horizontally, with several short connecting vertical fractures. In contrast, fractures in the fracture zones are generally orientated sub-vertically with short connecting sub-horizontal fractures. The fracture density in the fracture zones is an order of magnitude higher than in the massive gneiss (Table 1). Using NetworkGT (Nyberg et al., 2018), the fracture branches and nodes (intersections and fracture trace end-points) were characterised based on the topology of the branch intersections (Sanderson and Nixon, 2015). The massive gneiss is dominated by I-type nodes, whereas the fracture zones predominantly contain a combination of Y- and X-type nodes (Figure 4a-b; for node types see Figure 4g) (Table 1). Heat maps of intersection clustering from the massive gneiss versus a fracture zone illustrate the higher connectivity of the fracture zones. To quantify the connectivity across the Cauvery catchment area the connections per line and dimensionless intensity (a proxy for intensity that reflects average fracture

249   length) were calculated (following Sanderson and Nixon, 2015), (Table 1; Figure 4h). The connections,

250   i.e the number of X- and Y-nodes, per line length, is an indication of the percolation potential of a

251   fracture network (Sanderson and Nixon, 2018). The fracture zones have the highest connections per

252   line length and dimensionless intensity, suggesting they have the highest potential connectivity. In

253   contrast, the background gneiss has the lowest connections per line and intensity suggesting a relatively

254   low potential connectivity. The coefficient of variation (Cv) is calculated by dividing the standard

255   deviation of the fracture spacing by the mean fracture spacing (Gillespie et al., 1999; Watkins et al.,

256   2015b) and is used to quantify the how clustered a fracture network is (Table 1) (Odling et al., 1999).

257   The Cv ratios quantify the massive gneiss as generally having regularly-spaced fractures, while the

258   fractures in the fracture zones are highly clustered (Table 1, Figure 4h).

259

Rock type	Area (m²)	Mean length (m)	2D density (m⁻²)	I	U	X	Y	Dimensionless intensity	Connections per line	Coefficient of variation (Cv)
Fracture zone	4.6	0.2	17.8	157.0	61.0	121.0	517.0	3.3	3.8	1.4
Massive gneiss	15.0	0.6	1.4	41.0	10.0	1.0	11.0	0.8	0.9	0.2
Massive gneiss	11.9	1.0	1.9	19.0	15.0	0.0	10.0	1.9	1.4	0.6
Massive gneiss	26.8	0.5	3.9	136.0	32.0	18.0	157.0	2.0	2.4	0.8
Massive gneiss	8.5	0.3	8.8	130.0	40.0	38.0	204.0	2.7	2.9	1.3
Massive gneiss	137.8	2.9	0.7	21.0	10.0	6.0	23.0	1.9	2.6	0.9
Fracture zone	45.2	0.9	3.9	139.0	38.0	45.0	174.0	3.4	2.8	1.4
Fracture zone	38.5	1.7	1.6	139.0	38.0	45.0	174.0	2.6	2.8	1.3
Fracture zone	81.6	2.6	1.1	23.0	16.0	6.0	25.0	2.8	2.6	1.2
Massive gneiss	359.4	11.9	0.2	5.0	4.0	1.0	1.0	2.0	1.3	1.8
Massive gneiss	31.1	5.3	0.7	3.0	5.0	0.0	0.0	3.6	0.0	1.1
Fracture zone	9.2	1.5	1.4	4.0	6.0	0.0	6.0	2.1	2.4	0.7
Massive gneiss	13.3	2.1	0.9	2.0	8.0	0.0	2.0	1.9	2.0	0.5
Massive gneiss	10.5	1.9	0.9	2.0	5.0	2.0	1.0	1.7	4.0	0.7
Massive gneiss	119.6	2.1	0.8	41.0	12.0	4.0	27.0	1.6	1.8	0.4
Massive gneiss	95.4	2.3	1.0	29.0	19.0	5.0	30.0	2.4	2.4	0.5

260   **Table 1**: Summary fracture network statistics from the Peninsular Gneiss in the Cauvery Catchment,

261   southern India.

(a) Digital fracture traces on massive gneiss
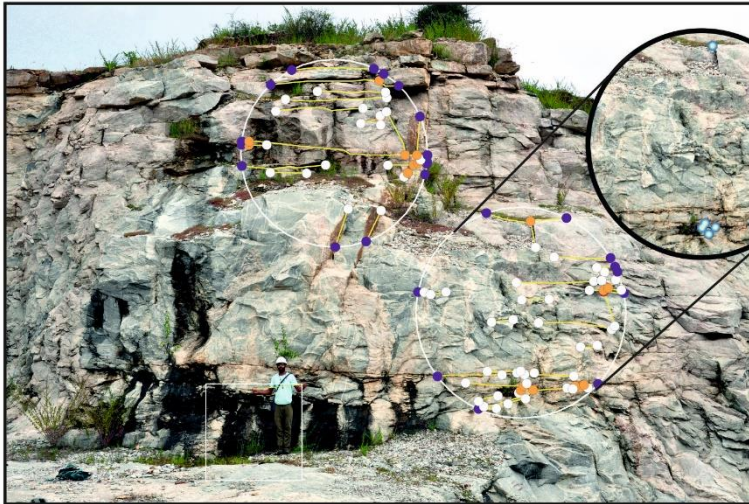
(c) Heat map of intersection density
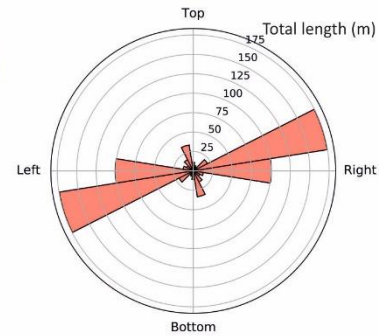
(e) Rose plot of fractures in background gneiss (n=176)

(b) Digital fracture traces from fracture zone

(d) Heat map of intersection density
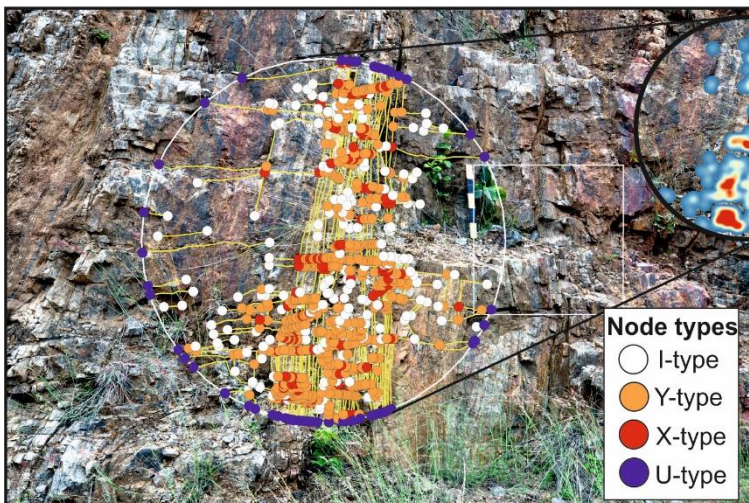
Node types
- I-type
- Y-type
- X-type
- U-type
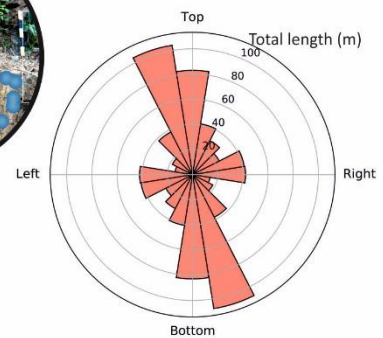
(f) Rose plot of fractures from fracture and shear zones (n=1104)

(g) Node types

I-type

Y-type

X-type

U-type (intersection with analysis window)
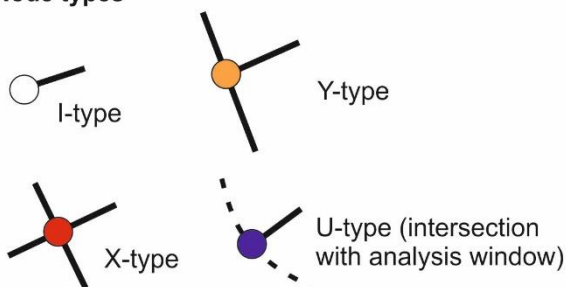
(h) Connectivity plot
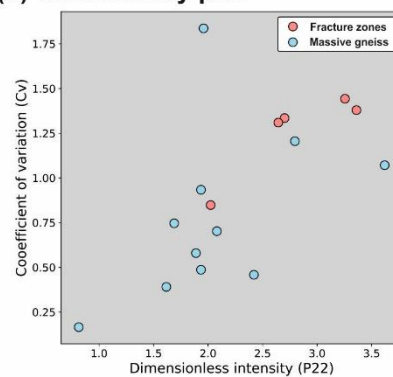
Fracture zones
Massive gneiss

262
263 **Figure 4**: Fracture analysis from the Peninsular Gneiss, South India, including: field photographs with
264 digitised fracture branches and intersection types on (a) a massive gneiss example; and (b) from a fracture
265 zone; (c-d) heat maps illustrate variations in fracture intersection density (massive gneiss: 0-5 nodes/m^2
266 and fracture zones: 0-18 nodes/m^2); (e-f) length-weighted rose plots showing the variation in orientation
267 of fractures traces in the background gneiss and fracture zones; (g) a schematic illustration of the various
268 types of fracture connections (as defined by Manzocchi, 2002); (h) a plot of connections per line against
269 dimensionless intensity (defined by Sanderson and Nixon, 2015) to show variations in connectivity.

270

At the near-surface, the Peninsular Gneiss has a bimodal fracture density distribution with fracture zones with high fracture density that make up a relatively small proportion of the bedrock, and the majority of the crystalline basement containing a low-density fracture pattern. Connectivity proxies, such as connections per line, indicate that the fracture zones have the highest potential permeability, whereas the permeability potential of the background gneiss is highly variable but still significantly lower.

In this case study, field time was limited and the digital method provided a quick and flexible way of gathering fracture network data. It was possible to carry out a reconnaissance survey covering an area over 30,000 km^2 and then retrospectively select the most suitable sites for fracture analysis. Key fracture parameters such as fracture length, orientation and density, which impacts on aquifer characteristics such as connectivity and permeability across the Peninsular Gneiss in the Cauvery River catchment, where then calculated and used to constrain local and regional-scale groundwater models (Collins et al. 2020).

3.2 Rock mass strength estimates (Geological Strength Index)

Structural discontinuities are an important control on the engineering behaviour of a rock mass (Müller, 1974; Hoek 1983, Hoek & Brown 1997). Slopes, foundations and shallow underground excavations in hard rock can be strongly be affected by the presence of discontinuities, for example, the intersection of structural features can lead to falling and sliding of blocks or wedges from the surface.

In the last decade, rock mass classification systems have been applied extensively in engineering design and construction (Liu, 2007). The Geological Strength Index (GSI) system provides a numerical representation of the overall geotechnical properties of a rock mass, which is estimated using a standard matrix chart and field observations of (a) the 'blockiness' of a rock mass and (b) the surface conditions of any discontinuities. The GSI Index is based upon an assessment of the lithology, structure and condition of discontinuity surfaces in the rock mass and it is estimated from visual examination of the rock mass exposed in surface excavations such as roadcuts, in tunnel faces and in borehole core (Marinos and Hoek, 2000). Both the 'blockiness' and surface conditions, however, are determined in a qualitative and descriptive manner, which is subjective and dependent on the interpreter. Sönmez and Ulusay (1999; 2002) suggested that the 'blockiness' or Structure Rating can be quantified by using the Volumetric Joint (fracture) Count (Jv, in m^{-1}). This parameter is defined as the sum of the number of joints per meter for each joint set present (Sönmez & Ulusay, 1999), and can be estimated by the following expression:

$$Jv = \frac{1}{S1} + \frac{1}{S2} + \cdots \frac{1}{Sn} \qquad (3)$$

305

306 where *S* is the spacing of the joints in a set and *n* is the number of joint sets. The 2D fracture digitisation

307 method can clearly be applied to determine a more accurate representation of Jv from an image.

308

309 The procedure for quantifying rock mass strength parameters in jointed rocks is illustrated using

310 massive and fractured gneiss exposures in India (Figure 4). Using the qualitative method (Hoek, 1983)

311 the massive gneiss, with 'good' fracture surfaces, has a GSI index of 70-85 whereas the fractured gneiss,

312 with 'fair' fracture surfaces, has a GSI index of 30-45. To quantify this, the modified GSI methodology

313 after Sönmez & Ulusay (1999) is used. In this example, the massive gneiss has horizontal joint spacing

314 of 0.81 m (J1) and vertical joint spacing of 6.19 m (J2). The fractured gneiss has a horizontal joint

315 spacing of 0.17 m (J1) and vertical joint spacing of 0.08 m (J2). Thus, using equation 3, this gives a Jv

316 value of 1.4 for the massive gneiss and 17.7 for the fractured gneiss. Based on similar estimates of

317 roughness (5), weathering (3) and infill (6) the fracture surface condition rating (SCR) is 14 in both the

318 massive gneiss and the fracture zones. Finally, the GSI values calculated are *c*. 76 for the massive gneiss

319 and only *c*. 44 for the fractured gneiss, demonstrating an accurate representation of the rock mass

320 strength differences of the massive and fractured gneiss.

321 When determining rock mass strength properties the digital method can provide a fast, accurate and

322 consistent result. Understanding rock mass strength properties is relevant for both academic and

323 industry users, in both cases, available field time can often be limited. In addition, particularly in

324 industry there is likely to be multiple interpreters making rock mass strength estimates, and therefore

325 this method can help improve consistency in the results by undertaking analysis digitally.

326

327 **3.3 Block size and rock erodibility, Southern Scotland**

328 Fracturing is a significant factor in the preconditioning of rock masses for erosion at the Earth's surface

329 (e.g. Roy et al., 2016; Clarke and Burbank, 2010). As well as influencing the volume of material

330 available for mobilisation and transport, fracturing of bedrock is a key control on the clast size

331 distribution of eroded material entering geomorphic systems from hillslopes, particularly in upland

332 landscapes (e.g. Sklar et al. 2016).

333 The 2D fracture digitisation method is here used to assess the spatial distribution of block-size and

334 fracture intensity of metasandstone of low metamorphic grade in the Southern Uplands, southern

335 Scotland. Block density can be expressed as blocks per square metre, which is easily derived from a

336 polygonised set of fracture traces. It should be noted that whether this 2D block size measure is

337 representative for the true 3D block size depends on the anisotropy of the fracture system and the

338 average block shape. Despite consistent bedrock type (metasandstone) across the study area, the

339 anisotropic fracture pattern gives rise to strong variations in block-size as shown by variation in the

340 number of blocks sampled per unit measuring area from <50 to >1000 blocks per m^2 (Figure 5). This

341 data can help to quantify key controls on the influence of facture intensity on block size, which may be

342 used to inform modelling erosion and sediment movement within landscapes.

343
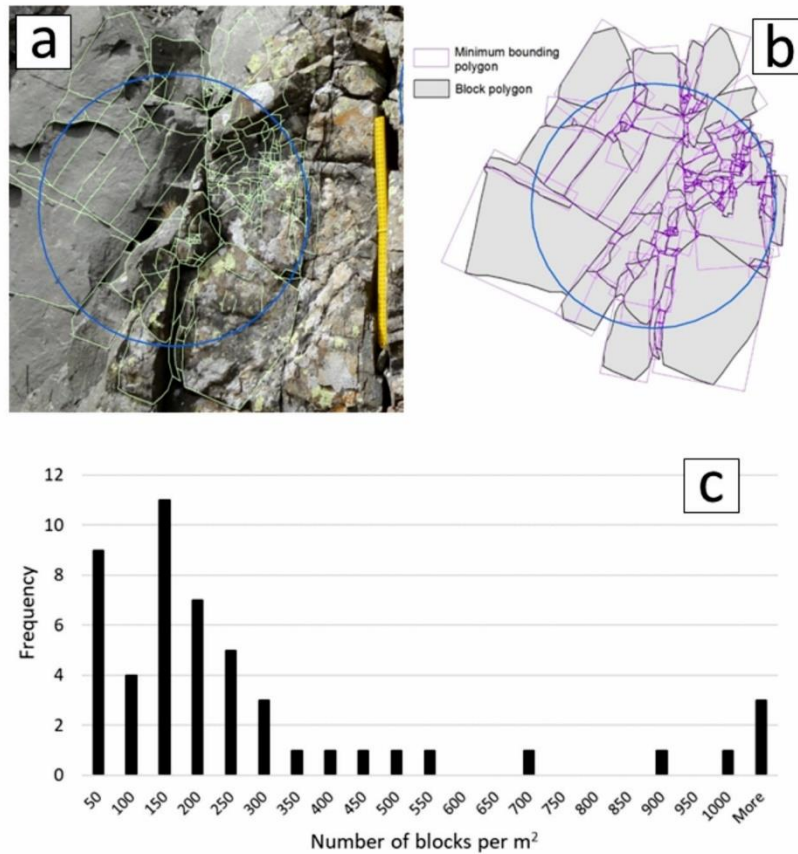
Figure 5. Derivation of block-size metrics for Wacke sandstone in the Southern Uplands of Scotland. Field
345 photograph of sandstone outcrop with fracture delineation (a), polygons for blocks sampled by the circular
346 window (b), number of blocks sampled per m^2 for dataset of 50 measuring sites from the study area.

347

348 For this study, a large amount of fracture and block data was required from several outcrops, and the

349 digital method provided an accurate and efficient way for gathering large amounts of fracture and block

350 size data. Due to the requirements of the study, photographs were taken close to the outcrop to improve

351 the accuracy of digitisation (Figure 5a), resulting in a large and accurate dataset.

3.4 Case studies summary

353 The case studies presented here demonstrate the broad range of benefits of a digital method during both

354 data collection and data analysis phases. The Cauvery Catchment case study demonstrates how the

355 digital method provided flexibility to gather data while on a short reconnaissance-style field-campaign,

356 with fracture data collected retrospectively from photographs taken at key localities. The digital dataset

357 allows for further evolved quantitative and graphical data analysis, such as heat maps of fracture

358 intersections to better understand connectivity. For engineering geology purposes, the digital method is

359 shown to provide a more accurate and consistent representation of the geological strength index (GSI)

360 of a rock mass. We build upon the well-used method for estimating GSI (Hoek, 1983; Sönmez &

361 Ulusay, 1999), to calculate a more accurate GSI based on fractures exposed in outcrop. Finally, the

362 block size and erodibility case study is used to demonstrate the benefits of being able to rapidly generate

363 a large digital dataset that would otherwise be impractical to gather in the field.

364 4 Advantages and disadvantages

365 The digital method described here is not meant to replace field-based data gathering but used in

366 conjunction, as it may be more suitable for different purposes. There are a number of advantages to

367 using a digital method for gathering fracture data including: speed of gathering data, creating large

368 datasets, flexibility in data gathering approach and consistency of data.

369 Gathering 2D fracture network data in the field can often be a time consuming processes and therefore

370 limits the amount of data that can be gathered during a field campaign. Using the digital methodology

371 allows for fracture network data to be quickly gathered in the office, allowing for more data to be

372 generated from an equivalent amount of time in the field. Field time can be used for detailed study of

373 the outcrop to improve the interpretation of fractures in the office and to gather other key data such as

374 aperture, fracture fill and 3D geometry's. The digital method allows for large, statistically significant

375 datasets to be quickly gathered during a short field campaign. Collecting the data after fieldwork with

376 a broader perspective provides an element of flexibility in terms of the selecting of outcrops for analysis,

377 the type and shape of the sample window and the amount of the data gathered. Finally, the digital

378 method has the potential to be used to improve the consistency and reliability of industry standards that

379 involve fracture networks, such as rock mass strength estimates (Section 3.2) by reducing collector bias

380 by standardising the data collection strategy.

381 For more evolved analysis of the fracture data the digital traces can be used in fracture analysis software

382 packages such as FracPaQ (Healy et al., 2017), NetworkGT (Nymberg et al., 2018), FraNEP (Zeeb et

383 al., 2013) and DigiFract (Hardebol and Bertotti 2013). These programmes can be used for wide range

384 of types of fracture analysis including topological analysis such as deducing node types, and plotting

385 fracture density heat maps illustrating density variations across a fracture zone.

386 There are limitations with capturing the data digitally. Firstly, capturing data in the field will always be

387 more reliable in terms of seeing the full extent of fractures: for example, fractures may be obscured by

388 vegetation making digitisation of traces more difficult than in the field (Andrews et al., 2019). Secondly,

389 field observations of the character of individual fractures such as roughness, aperture and any secondary

390 fills can be important observations made only in the field and useful when understanding rock mass

391 strength or permeability. It is also possible, of course, to digitise the fracture network, and then return

392 to the outcrop and augment the digital traces with further attribution that requires direct field observation

393 (e.g. fracture aperture, fracture fill); portable PC tablets are ideal for this purpose. Image scale can also

394 be an issue with this method, as smaller fractures can be harder to digitise from a from a single
395 photograph covering a large outcrop extent, therefore it is important to acquire photographs that cover
396 the appropriate scale of fractures, which will be dependent on the purpose of the study. Estimates of
397 fracture permeability and percolation when using topology alone represent the maximum potential and
398 does not account of closed fractures (Laubach et al., 2019). Additional observations such as aperture
399 and infilling are import for these types of studies.

400 Characterising the architecture of a fracture network is useful for understanding relative age history of
401 fracture sets, this can be significant when making larger scale interpretations particularly for fluid flow
402 modelling (Hancock 1985; Peacock et al 2018). Relative age relationships are best determined in the
403 field and can be challenging to gather digitally. It is important to appreciate the limitations of the
404 method, as it may not be suitable for all studies or may need supplementary field data.

405 **5 Conclusions**

406 The aim of this paper is to review and evaluate the methodology for digitising 2D fracture networks in
407 GIS, and make it more accessible to a broader range of users in both academia and industry. We present
408 a breakdown of the key steps in the methodology, which provides an understanding of how to avoid
409 error and improve the accuracy of the final dataset.

410 The digital method can be used to interpret traces of 2D linear features of a wide variety of scales from
411 the local metre-scale to the kilometre scale, including, fractures at outcrop scale to regional-scale
412 structural lineaments that are visible on aerial photographs or DEMs.

413 An important aspect of applied geosciences, such as hydrogeology and geotechnical engineering is the
414 accurate parameterisation of fracture networks in bedrock. The methodology that is commonly used is
415 a qualitative description and can be time consuming. The digital 2D fracture trace capture method is an
416 accurate and rapid way of quantifying 2D linear networks such as fracture zones using open access
417 software packages. It offers a robust, cost-effective methodology that can used in academy and industry
418 to gather accurate 2D fracture network data.

419 **Acknowledgements**

420 This paper was supported by the British Geological Survey NC-ODA grant NE/R000069/1: *Geoscience*
421 *for Sustainable Futures* and is published with the permission of the Executive Director of the Geological
422 Survey. Martin Gillespie is thanked for helpful comments on the manuscript. The paper has benefited
423 from detailed comments from Francesco Mazzarini and two anonymous reviewers.

424

425

426 **References**

427 Andrews, B. J., Roberts, J. J., Shipton, Z. K., Bigi, S., Tartarello, M. C., and Johnson, G.: How do we
428   see fractures? Quantifying subjective bias in fracture data collection, Solid Earth, 10, 487-516,
429   2019.

430 Bandpey, A. K., Shahriar, K., Sharifzadeh, M., and Marefvand, P.: Comparison of methods for
431   calculating geometrical characteristics of discontinuities in a cavern of the Rudbar Lorestan
432   power plant, Bulletin of Engineering Geology and the Environment, 1-21, 2017.

433 Barton, N., Lien, R., and Lunde, J.: Engineering classification of rock masses for the design of tunnel
434   support, Rock mechanics, 6, 189-236, 1974.

435 Bieniawski, Z. T.: Rock mechanics design in mining and tunnelling, Monograph, 1984.

436 Bieniawski, Z. T., and Bieniawski, Z.: Engineering rock mass classifications: a complete manual for
437   engineers and geologists in mining, civil, and petroleum engineering, John Wiley & Sons, 1989.

438 Clarke, B. A., and Burbank, D. W.: Bedrock fracturing, threshold hillslopes, and limits to the magnitude
439   of bedrock landslides, Earth and Planetary Science Letters, 297, 577-586, 2010.

440 Collins, S. L., Loveless, S. E., Muddu, S., Buvaneshwari, S., Palamakumbura, R. N., Krabbendam, M.,
441   Lapworth, D. J., Jackson, C. R., Gooddy, D. C., and Nara, S. N. V.: Groundwater connectivity
442   of a sheared gneiss aquifer in the Cauvery River basin, India,

443 Davis, G. H., Reynolds, S. J., and Kluth, C. F.: Structural geology of rocks and regions, John Wiley &
444   Sons, 2011.

445 Dühnforth, M., Anderson, R. S., Ward, D., and Stock, G. M.: Bedrock fracture control of glacial erosion
446   processes and rates, Geology, 38, 423-426, 2010.

447 Follin, S., Hartley, L., Rhén, I., Jackson, P., Joyce, S., Roberts, D., and Swift, B.: A methodology to
448   constrain the parameters of a hydrogeological discrete fracture network model for sparsely
449   fractured crystalline rock, exemplified by data from the proposed high-level nuclear waste
450   repository site at Forsmark, Sweden, Hydrogeology Journal, 22, 313-331, 2014.

451 Gillespie, P., Johnston, J., Loriga, M., McCaffrey, K., Walsh, J., and Watterson, J.: Influence of layering
452   on vein systematics in line samples, Geological Society, London, Special Publications, 155, 35-
453   56, 1999.

454 Guihéneuf, N., Boisson, A., Bour, O., Dewandel, B., Perrin, J., Dausse, A., Viossanges, M., Chandra,
455   S., Ahmed, S., and Maréchal, J.: Groundwater flows in weathered crystalline rocks: Impact of
456   piezometric variations and depth-dependent fracture connectivity, Journal of Hydrology, 511,
457   320-334, 2014.

458 Hancock, P.: Brittle microtectonics: principles and practice, Journal of structural geology, 7, 437-457,
459   1985.

Hardebol, N., and Bertotti, G.: DigiFract: A software and data model implementation for flexible acquisition and processing of fracture data from outcrops, Computers & Geosciences, 54, 326-336, 2013.

Healy, D., Rizzo, R. E., Cornwell, D. G., Farrell, N. J., Watkins, H., Timms, N. E., Gomez-Rivas, E., and Smith, M.: FracPaQ: A MATLAB™ toolbox for the quantification of fracture patterns, Journal of Structural Geology, 95, 1-16, 2017.

Hoek, E.: Strength of jointed rock masses, Geotechnique, 33, 187-223, 1983.

Hoek, E., and Brown, E. T.: Practical estimates of rock mass strength, International journal of rock mechanics and mining sciences, 34, 1165-1186, 1997.

Hong, K., Han, E., and Kang, K.: Determination of geological strength index of jointed rock mass based on image processing, Journal of Rock Mechanics and Geotechnical Engineering, 9, 702-708, 2017.

Hooyer, T. S., Cohen, D., and Iverson, N. R.: Control of glacial quarrying by bedrock joints, Geomorphology, 153, 91-101, 2012.

Krabbendam, M., and Glasser, N. F.: Glacial erosion and bedrock properties in NW Scotland: abrasion and plucking, hardness and joint spacing, Geomorphology, 130, 374-383, 2011.

Krabbendam, M., and Bradwell, T.: Quaternary evolution of glaciated gneiss terrains: pre-glacial weathering vs. glacial erosion, Quaternary Science Reviews, 95, 20-42, 2014.

Krabbendam, M., Eyles, N., Putkinen, N., Bradwell, T., and Arbelaez-Moreno, L.: Streamlined hard beds formed by palaeo-ice streams: A review, Sedimentary Geology, 338, 24-50, 2016.

Laubach, S. E., Lamarche, J., Gauthier, B. D., Dunne, W. M., and Sanderson, D. J.: Spatial arrangement of faults and opening-mode fractures, Journal of Structural Geology, 108, 2-15, 2018.

Laubach, S. E., Lander, R., Criscenti, L. J., Anovitz, L. M., Urai, J., Pollyea, R., Hooker, J. N., Narr, W., Evans, M. A., and Kerisit, S. N.: The role of chemistry in fracture pattern development and opportunities to advance interpretations of geological materials, Reviews of Geophysics, 57, 1065-1111, 2019.

Liu, Y.-C., and Chen, C.-S.: A new approach for application of rock mass classification on rock slope stability assessment, Engineering geology, 89, 129-143, 2007.

Mahé, S., Gasc-Barbier, M., and Soliva, R.: Joint set intensity estimation: comparison between investigation modes, Bulletin of Engineering Geology and the Environment, 74, 171-180, 2015.

Mäkel, G.: The modelling of fractured reservoirs: Constraints and potential for fracture network geometry and hydraulics analysis, Geological Society, London, Special Publications, 292, 375-403, 2007.

Manzocchi, T.: The connectivity of two-dimensional networks of spatially correlated fractures, Water Resources Research, 38, 1-1-1-20, 2002.

495 Maréchal, J.-C., Dewandel, B., Ahmed, S., Galeazzi, L., and Zaidi, F. K.: Combined estimation of
496   specific yield and natural recharge in a semi-arid groundwater basin with irrigated agriculture,
497   Journal of Hydrology, 329, 281-293, 2006.

498 Marinos, P., and Hoek, E.: GSI: a geologically friendly tool for rock mass strength estimation, ISRM
499   international symposium, 2000,

500 Mauldon, M., Dunne, W., and Rohrbaugh Jr, M.: Circular scanlines and circular windows: new tools
501   for characterizing the geometry of fracture traces, Journal of Structural Geology, 23, 247-258,
502   2001.

503 Menegoni, N., Giordan, D., Perotti, C., and Tannant, D. D.: Detection and geometric characterization
504   of rock mass discontinuities using a 3D high-resolution digital outcrop model generated from
505   RPAS imagery–Ormea rock slope, Italy, Engineering geology, 252, 145-163, 2019.

506 Müller, L.: Rock mechanics, Springer, 1974.

507 Nyberg, B., Nixon, C. W., and Sanderson, D. J.: NetworkGT: A GIS tool for geometric and topological
508   analysis of two-dimensional fracture networks, Geosphere, 14, 1618-1634, 2018.

509 Odling, N., Gillespie, P., Bourgine, B., Castaing, C., Chiles, J., Christensen, N., Fillion, E., Genter, A.,
510   Olsen, C., and Thrane, L.: Variations in fracture system geometry and their implications for fluid
511   flow in fractures hydrocarbon reservoirs, Petroleum Geoscience, 5, 373-384, 1999.

512 Park, H.-J., West, T. R., and Woo, I.: Probabilistic analysis of rock slope stability and random properties
513   of discontinuity parameters, Interstate Highway 40, Western North Carolina, USA, Engineering
514   Geology, 79, 230-250, 2005.

515 Peacock, D., Nixon, C., Rotevatn, A., Sanderson, D., and Zuluaga, L.: Glossary of fault and other
516   fracture networks, Journal of Structural Geology, 92, 12-29, 2016.

517 Peacock, D., Dimmen, V., Rotevatn, A., and Sanderson, D.: A broader classification of damage zones,
518   Journal of Structural Geology, 102, 179-192, 2017.

519 Peacock, D., Sanderson, D., and Rotevatn, A.: Relationships between fractures, Journal of Structural
520   Geology, 106, 41-53, 2018.

521 Perrin, J., Ahmed, S., and Hunkeler, D.: The effects of geological heterogeneities and piezometric
522   fluctuations on groundwater flow and chemistry in a hard-rock aquifer, southern India,
523   Hydrogeology Journal, 19, 1189, 2011.

524 Pless, J.: Characterising fractured basement using the Lewisian Gneiss Complex, NW Scotland:
525   implications for fracture systems in the Clair Field basement, Durham University, 2012.

526 Pless, J., McCaffrey, K., Jones, R., Holdsworth, R., Conway, A., and Krabbendam, M.: 3D
527   characterization of fracture systems using terrestrial laser scanning: An example from the
528   Lewisian basement of NW Scotland, Geological Society, London, Special Publications, 421,
529   125-141, 2015.

530 Procter, A., and Sanderson, D. J.: Spatial and layer-controlled variability in fracture networks, Journal
531   of Structural Geology, 108, 52-65, 2018.

532 Ren, F., Ma, G., Fan, L., Wang, Y., and Zhu, H.: Equivalent discrete fracture networks for modelling
533   fluid flow in highly fractured rock mass, Engineering geology, 229, 21-30, 2017.

534 Rizzo, R. E., Healy, D., and De Siena, L.: Benefits of maximum likelihood estimators for fracture
535   attribute analysis: Implications for permeability and up-scaling, Journal of Structural Geology,
536   95, 17-31, 2017.

537 Roy, S., Tucker, G., Koons, P., Smith, S., and Upton, P.: A fault runs through it: Modeling the influence
538   of rock strength and grain-size distribution in a fault-damaged landscape, Journal of Geophysical
539   Research: Earth Surface, 121, 1911-1930, 2016.

540 Sanderson, D. J., and Nixon, C. W.: The use of topology in fracture network characterization, Journal
541   of Structural Geology, 72, 55-66, 2015.

542 Sanderson, D. J., and Nixon, C. W.: Topology, connectivity and percolation in fracture networks,
543   Journal of Structural Geology, 115, 167-177, 2018.

544 Selby, M. J.: Hillslope materials and processes, Hillslope materials and processes., 1982.

545 Singhal, B. B. S., and Gupta, R. P.: Applied hydrogeology of fractured rocks, Springer Science &
546   Business Media, 2010.

547 Sklar, L. S., Riebe, C. S., Marshall, J. A., Genetti, J., Leclere, S., Lukens, C. L., and Merces, V.: The
548   problem of predicting the size distribution of sediment supplied by hillslopes to rivers,
549   Geomorphology, 277, 31-49, 2017.

550 Sonmez, H., and Ulusay, R.: Modifications to the geological strength index (GSI) and their applicability
551   to stability of slopes, International Journal of Rock Mechanics and Mining Sciences, 36, 743-
552   760, 1999.

553 Sonmez, H., and Ulusay, R.: A discussion on the Hoek-Brown failure criterion and suggested
554   modifications to the criterion verified by slope stability case studies, Yerbilimleri, 26, 77-99,
555   2002.

556 Stober, I., and Bucher, K.: Hydraulic properties of the crystalline basement, Hydrogeology Journal, 15,
557   213-224, 2007.

558 Strijker, G., Bertotti, G., and Luthi, S. M.: Multi-scale fracture network analysis from an outcrop
559   analogue: A case study from the Cambro-Ordovician clastic succession in Petra, Jordan, Marine
560   and Petroleum Geology, 38, 104-116, 2012.

561 Sturzenegger, M., Sartori, M., Jaboyedoff, M., and Stead, D.: Regional deterministic characterization
562   of fracture networks and its application to GIS-based rock fall risk assessment, Engineering
563   geology, 94, 201-214, 2007.

564 Sturzenegger, M., Stead, D., and Elmo, D.: Terrestrial remote sensing-based estimation of mean trace
565   length, trace intensity and block size/shape, Engineering Geology, 119, 96-111, 2011.

566 Tavani, S., Corradetti, A., and Billi, A.: High precision analysis of an embryonic extensional fault-
567   related fold using 3D orthorectified virtual outcrops: The viewpoint importance in structural
568   geology, Journal of Structural Geology, 86, 200-210, 2016.

569 Thiele, S. T., Grose, L., Samsu, A., Micklethwaite, S., Vollgger, S. A., and Cruden, A. R.: Rapid, semi-
570 automatic fracture and contact mapping for point clouds, images and geophysical data, Solid
571 Earth, 8, 1241, 2017.

572 Ukar, E., Laubach, S. E., and Hooker, J. N.: Outcrops as guides to subsurface natural fractures: Example
573 from the Nikanassin Formation tight-gas sandstone, Grande Cache, Alberta foothills, Canada,
574 Marine and Petroleum Geology, 103, 255-275, 2019.

575 Vasuki, Y., Holden, E.-J., Kovesi, P., and Micklethwaite, S.: Semi-automatic mapping of geological
576 Structures using UAV-based photogrammetric data: An image analysis approach, Computers &
577 Geosciences, 69, 22-32, 2014.

578 Voorn, M., Exner, U., Barnhoorn, A., Baud, P., and Reuschlé, T.: Porosity, permeability and 3D fracture
579 network characterisation of dolomite reservoir rock samples, Journal of Petroleum Science and
580 Engineering, 127, 270-285, 2015.

581 Watkins, H., Bond, C. E., Healy, D., and Butler, R. W.: Appraisal of fracture sampling methods and a
582 new workflow to characterise heterogeneous fracture networks at outcrop, Journal of Structural
583 Geology, 72, 67-82, 2015a.

584 Watkins, H., Butler, R. W., Bond, C. E., and Healy, D.: Influence of structural position on fracture
585 networks in the Torridon Group, Achnashellach fold and thrust belt, NW Scotland, Journal of
586 Structural Geology, 74, 64-80, 2015b.

587 Zeeb, C., Gomez-Rivas, E., Bons, P. D., and Blum, P.: Evaluation of sampling methods for fracture
588 network characterization using outcrops, AAPG bulletin, 97, 1545-1566, 2013.

589 Zeeb, C., Gomez-Rivas, E., Bons, P. D., Virgo, S., and Blum, P.: Fracture network evaluation program
590 (FraNEP): A software for analyzing 2D fracture trace-line maps, Computers & geosciences, 60,
591 11-22, 2013.

592 Zhan, J., Xu, P., Chen, J., Wang, Q., Zhang, W., and Han, X.: Comprehensive characterization and
593 clustering of orientation data: A case study from the Songta dam site, China, Engineering
594 geology, 225, 3-18, 2017.

595